International Journal of Mass Spectrometry and Ion Processes, 54 (1983) 169–187
Elsevier Science Publishers B.V., Amsterdam – Printed in The Netherlands

THEORY OF SPACE-CHARGE SHIFT OF ION CYCLOTRON RESONANCE FREQUENCIES

J.B. JEFFRIES *, S.E. BARLOW and G.H. DUNN †

Joint Institute for Laboratory Astrophysics, University of Colorado and National Bureau of Standards, Boulder, CO 80309 (U.S.A.)

(Received 29 March 1983)

ABSTRACT

A theory of ion space-charge influence on the observed ion cyclotron resonance frequency in static field ion traps is presented. The dependence of this influence on ion density, ion cloud shape, and trapping geometry is investigated. Four trapping geometries are specifically analyzed: the Penning trap, the cubical ICR cell, the common rectangular ICR cell, and an elongated ICR cell. This treatment is readily extended to other geometries. The theory applies to common situations where the exciting or detecting antennae fields are not homogeneous, and individual particle motions are excited/detected as opposed to center-of-mass motions.

INTRODUCTION

The storage of charged particles in an electrostatic potential well and a strong static magnetic field has proven to be a useful technique for the study of a wide variety of physical phenomena since first used by Penning to investigate gas discharges [1]. Static field ion traps, called ion cyclotron resonance (ICR) cells, have been used extensively in chemical physics for the gas-phase study of ion/molecule reactions and selected reviews of this literature are noted [2–4]. The ions stored in these instruments are detected by resonance with the eigenfrequency near the ion cyclotron frequency, $\omega_c = qB/m$, where q is the ion charge, B is the magnetic field and m is the ion mass.

Ion cyclotron resonance cells have also been used successfully for precision mass spectroscopy. Careful work by McIver and coworkers [5,6] generated an absolute mass calibration for a mixture of 12 masses ranging from 46–264 u with an average error of 77 p.p.m. They also noted in this work a

* Present address: Chemistry Dept., University of Pittsburgh, Pittsburgh, PA 15260.
† Staff Member, Quantum Physics Division, National Bureau of Standards.

0168-1176/83/$03.00

shift in the resonance frequency as ions were ejected from the trap. Ledford et al. [7] empirically fitted the ion number dependence for a specific set of experimental conditions and obtained a better (3 p.p.m.) absolute ion mass calibration. Introduction of the Fourier transform detection technique [8–10] which does not eject ions on detection, has made considerable improvements in resolution ($M/\Delta M \cong 10^5$), which has been exploited by Ledford et al. [7], and also promises even more improvement in ICR precision mass spectroscopy. It has become clear, however, that to realize fully the potential of this mass spectroscopic technique for high accuracy, a more complete understanding of the effects of space-charge must be developed. Using the advanced ICR techniques alluded to above and the space-charge corrections developed in this paper, Francl et al. [11] have made mass determinations with average errors less than 1 p.p.m.

On the other hand, Wineland et al. [12] have achieved conservatively estimated uncertainties of 0.34 p.p.m. in a mass determination using a Penning trap and laser-fluorescence mass spectroscopy, operating in such a manner that no corrections were needed for space-charge or other ion number effects. They project ultimate accuracies of near 1 part in 10^{13}. It has been emphasized by Wineland and Dehmelt [13,14] that the space-charge associated with an ion cloud consisting of particles of a single charge-to-mass ratio, q/M, cannot and does not influence the center-of-mass motion of the cloud. Thus, if the antennae used to excite the ions or to detect them interact only with the center-of-mass, there will be no shift of the observed resonant frequencies. Such, for example, is the case for ions confined very near to the center of a Penning trap, or for other cases where the exciting or probe fields may be considered homogeneous. These "no shift" situations have been achieved for charged particle clouds of a single q/M [15]. However, for most ICR work and for the work we have done with Penning traps where ion cloud radii are moderate, the antennae fields are not homogeneous, and one is dealing with the frequencies of individual ions in net fields originating from those impressed and those from surrounding ions. It is such situations to which the analysis of this paper is addressed and to which the derived corrections should be applied.

Recent investigations [16] into the dynamics of trapped ions have led to a greater insight into the behavior of ion clouds in static field traps. These investigations were motivated by work with electron–ion collisions [17–19] and low temperature ion/neutral species reactions [20]. From this work a more detailed model of the ion cyclotron resonance frequency has emerged, which includes the contribution of ion space-charge. This model is applicable not only to the highly accurate quadrupole fields of our systems, but also to the cubical and rectangular geometries of widely used ICR cells.

Four ion trap geometries will be considered, all currently used in ion trap

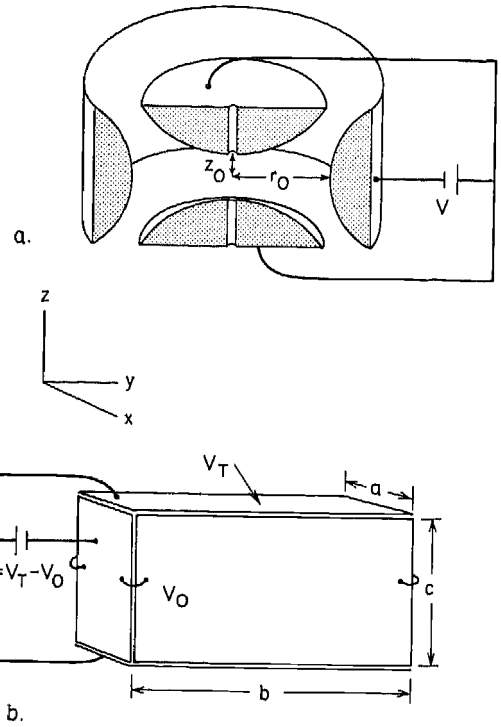

Fig. 1. Ion electrode trap geometries: (a) "Penning" trap, dimensions r_0, z_0; (b) general ICR geometry, dimensions a, b, c (x, y, z).

instruments, each of which uses a strong static uniform magnetic field that is oriented in the positive z direction. The magnetic field assumed to be aligned along the z axis confines the ions radially, and an applied electrostatic potential confines the ions in the z direction. The various trap configurations discussed here are illustrated in Fig. 1. Figure 1(a) depicts the "Penning" trap first analyzed by Byrne and Fargo [21] for electrons, and currently used for a wide variety of spectroscopy, metrology, and atomic collisions applications [15–20,22–26]. This trap is cylindrically symmetric, and the trapping electrodes (two end caps and a ring) are carefully machined along equipotentials of the saddle potential given in cylindrical coordinates by

$$V(r, z) = VG_T\left(-r^2 + 2z^2 + r_0^2\right) \tag{1}$$

where G_T is a trap geometry factor, $G_T = 1/(r_0^2 + 2z_0^2)$, r_0 and z_0 are characteristic dimensions shown in Fig. 1(a), and V is the potential applied between the two end cap electrodes and the ring electrode.

Figure 1(b) depicts a general ICR cell where the x, y and z dimensions are given by a, b and c, respectively. The two most widely used ICR cells have

cubical ($a = b = c$) and rectangular ($a = c < b$) geometries. An elongated cell ($a = b < c$) introduced recently by Hunter et al. [27] has many advantages for mass spectrometry over conventional ICR cells. The exact electrostatic potentials produced by the rectangular flat plate electrodes common to all the ICR cells is given [28] in Cartesian coordinates by

$$V(x,y,z) = V_0 - 16\pi^2(V_T - V_0) \times \sum_{m=0}^{\infty}\sum_{n=0}^{\infty} \frac{\cosh\left(k_{mn}\frac{\pi}{c}z\right)(-1)^{m+n}\cos\left[(2m+1)\frac{\pi x}{a}\right]\cos\left[(2n+1)\frac{\pi y}{b}\right]}{\cosh(k_{mn}\pi/2)(2m+1)(2n+1)} \tag{2}$$

where V_0 and V_T are applied electric potentials shown in Fig. 1(b). In all of the ICR geometries, it can be shown that the potentials are essentially harmonic in a large region near the center of each cell and are closely approximated by [7,27,28]

$$V(x,y,z) = \frac{1}{2}(V_T + V_0) + (V_T - V_0)\left[-\frac{\alpha}{a^2}x^2 - \frac{\beta}{b^2}y^2 + \left(\frac{\alpha}{a^2} + \frac{\beta}{b^2}\right)z^2 - \gamma\right] \tag{3}$$

TABLE 1

Geometric factors for various traps

Type	Dimensions (m)	α, β, γ [eqn. (3)]	G_T (m^{-2}) [eqn. (30)]	G_{T_x} (m^{-2}) (eqn. (42)]
Penning	$r_0 = 6.25\times10^{-3}$	1	$\frac{1}{r_0^2+2z_0^2} = 1.472\times10^4$	$\frac{2}{r_0^2+2z_0^2} = 2.942\times10^4$
	$z_0 = 3.8\times10^{-3}$			
Penning	$r_0 = 1.25\times10^{-2}$	1	$\frac{1}{r_0^2+2z_0^2} = 3.68\times10^3$	$\frac{2}{r_0^2+2z_0^2} = 7.36\times10^3$
	$z_0 = 7.6\times10^{-3}$			
Cubical	$l = 2.64\times10^{-2}$	$\alpha = 1.3869$		
ICR [7]		$\beta = 1.3869$	$\alpha/a^2 = 1.99\times10^3$	$\frac{2\alpha}{a^2} = 3.98\times10^3$
$a = b = c = l$		$\gamma = 0.1667$		
Elongated	$a = 3.2\times10^{-2}$	$\alpha = 4.183\times10^{-4}$		
ICR [27]	$b = 1.52\times10^{-1}$	$\beta = 4.183\times10^{-4}$	$\alpha/a^2 = 4.085\times10^{-1}$	$\frac{2\alpha}{a^2} = 8.170\times10^{-1}$
$a = b < c$		$\gamma = 0.500$		
Rectangular	$a = 2.54\times10^{-2}$	$\alpha = 2.185$	$G_{T_x} = \alpha/a^2 = 3.39\times10^3$	
ICR [28]	$b = 8.89\times10^{-2}$	$\beta = 8.27\times10^{-2}$		$G_{T_x} + G_{T_y} = 3.4\times10^3$
$a = c < b$			$G_{T_y} = \beta/b^2 = 1.05\times10^1$	
		$\gamma = 6.97\times10^{-4}$		

where α, β, and γ are constants depending on the specific dimensions of the ICR cell. Table 1 shows numerical values for the specific cases considered here. For simplicity we will take $V = V_T - V_0$ henceforth. From eqns. (1) and (3), the similarity between the "Penning" trap and the ICR cell becomes more apparent; the ions in both systems are trapped in a longitudinal magnetic and a harmonic electrostatic field. In fact, for the cubic cell ($a = b = c$) and the elongated cell ($a = b < c$), $\alpha = \beta$ and eqn. (3) reduces to eqn. (1).

SINGLE ION MOTION

The analysis of the motion of a single trapped ion will be considered here, thus establishing both the conceptual framework and the formalism to be used later in the inclusion of space-charge effects. Since we are concerned only with the resonance frequencies, it is noted that in the underdamped case, damping does not change the frequency at which the oscillator absorbs energy [29], thus there is no need to consider its effects further. The equations of motion are separable in z under the already stated assumption that the coordinates for B and E are colinear. This means that one can solve for the motions parallel and perpendicular to the magnetic field independently. The trajectory along the magnetic field is that for a simple harmonic oscillator of frequency

$$\omega_z = (2K_z)^{1/2} \tag{4}$$

where

$$K_z = 2qVG_{Tz}/m \tag{5}$$

and G_{Tz} is a trap geometric factor given in Table 1.

The motion in the x–y plane is also solvable in closed form for eqns. (1) and (3) when $\alpha = \beta$. In Cartesian coordinates the Lagrangian is written

$$L = \tfrac{1}{2}m(\dot{x}^2 + \dot{y}^2) + \tfrac{1}{2}mK(x^2 + y^2) + \tfrac{1}{2}m\omega_c(\dot{y}x - \dot{x}y) \tag{6}$$

where

$$K = 2qVG_T/m \tag{7}$$

and G_T is a trap geometric factor given in Table 1. Equation (6) leads to the coupled equations of motion

$$\ddot{x} - Kx - \omega_c\dot{y} = 0 \tag{8a}$$

$$\ddot{y} - Ky + \omega_c\dot{x} = 0 \tag{8b}$$

Applying the initial conditions of $x(0) = x_0$, $\dot{x}(0) = \dot{x}_0$, $y(0) = y_0$ and $\dot{y}(0) = \dot{y}_0$, and following the convention of Byrne and Fargo, $R \equiv x + iy$, the trajectory in the x–y plane is

$$R = \underline{a}e^{-i\omega_- t} - \underline{b}e^{-i\omega_+ t} \tag{9}$$

where

$$\underline{a} = \frac{1}{\omega_+ - \omega_-}\left[(\omega_+ x_0 - \dot{y}_0) + i(\omega_+ y_0 - \dot{x}_0)\right] \approx r_{gc} \tag{10a}$$

$$\underline{b} = \frac{1}{\omega_+ - \omega_-}\left[(\omega_- x_0 - \dot{y}_0) + i(\omega_- y_0 - \dot{x}_0)\right] \approx r_c \tag{10b}$$

in which r_{gc} is the guiding center radius, and r_c is the cyclotron radius. The eigenfrequencies are given by

$$\omega_- = \frac{\omega_c}{2}\left[1 - \left(1 - \frac{4K}{\omega_c^2}\right)^{1/2}\right] \tag{11}$$

for the slow drift (magnetron motion) around the z axis, and

$$\omega_+ = \frac{\omega_c}{2}\left[1 + \left(1 - \frac{4K}{\omega_c^2}\right)^{1/2}\right] \tag{12}$$

for the observed ICR frequency. Thus, the ion motion is the superposition of simple harmonic motion in the z direction at ω_z, a slow drift of the ions' guiding center about the z axis at ω_-, and the cyclotron motion about the guiding center at ω_+. Ekstrom and Wineland [30] graphically illustrate this motion.

These eigenfrequencies for single particle motion were deduced by Byrne and Fargo [21] for the Penning trap, and apply as well to ICR cells when $a = b$ (cubical and elongated). Equation (12) for ω_+ is identical to that of Hunter et al. [27]. It is also useful to compare the observed ICR frequency in eqn. (12) with the commonly used expression of Beauchamp and Armstrong [31]. They approximate the applied electrostatic potential by that between infinite parallel plates and thus neglect the coupling term, K_y, in eqn. (8b), obtaining

$$\omega \approx \left(\omega_c^2 - \omega_z^2\right)^{1/2} \tag{13}$$

In the limit $\omega_c \gg \omega_z$ and both eqns. (12) and (13) reduce to

$$\omega_+ \approx \omega \approx \omega_c - \frac{\omega_z^2}{2\omega_c} = \omega_c - \frac{2VG_T}{B} \tag{14}$$

The physics underlying the drift at frequency ω_- is straightforward. The

electrostatic potentials given in eqns. (1) and (3) give rise to an electric field with a radial component, $E_r = 2rVG_T$, which is perpendicular to the magnetic field. Therefore, an ion with a nonzero guiding center radius r_{gc} [eqn. (10a)] has a drift velocity about the z axis

$$v_D = \frac{EXB}{|B|^2} = \frac{2r_{gc}VG_T}{B}\hat{\theta} \tag{15}$$

Since $v_D \propto r$, this drift has definite frequency

$$\omega_m = \frac{|v_D|}{r} = \frac{2G_TV}{B} \tag{16}$$

and is called the magnetron frequency for historical reasons. Equation (11) for ω_- gives the same result when we expand using $\omega_c \gg \omega_m$. This approximation, though quite good, removes the weak mass dependence in eqn. (11) which ultimately sets the mass limits for trapping with given electric and magnetic fields.

SPACE-CHARGE EFFECTS

Reviewing eqns. (7)–(12), note that any radial electric field, $E = K'r$, will give the same result provided $K' < \omega_c^2/4$. We will show in this section that the principal effect of ion space-charge is to produce an additional radial electric field, thus changing K from a constant to a quantity K' dependent on charge density. Using the formalism and notation from the above development of single particle motion, we will proceed to include the contribution of ionic space-charge. Implicit in the following analysis is the assumption that the ion cloud can be characterized by a temperature that is low compared to the trapping potential energy. The dominant effects in the thermalization of the ion cloud are determined by the relative densities of ions and neutral species: for sufficiently low neutral densities the ion–ion coulombic collisions will establish a Maxwell–Boltzmann velocity distribution involving a temperature which may be significantly different from the background neutral temperature. The ion cloud will then interact with the neutral gas to establish an equilibrium state [16]. Alternatively, if the background density is sufficiently high, ion/neutral species collisions will dominate the thermalization process and the ions will approach a Maxwell–Boltzmann velocity distribution at about the same rate as they are cooled.

For cylindrically symmetric ion clouds with a radius r_P (Penning and $a = b$ ICR cells) the ion number density can be written [32] in terms of the

ion temperature, T_i, as

$$\rho(r,z)=\frac{\rho_0}{(2\pi mkT_i)^{3/2}}\int \mathrm{d}\underset{\sim}{p}\,\exp\left(-\frac{(H-P_\theta\omega_-)}{kT_i}\right) \quad r<r_P$$
$$\rho(r,z)\equiv 0 \qquad r>r_P \tag{17}$$

where H is the Hamiltonian, ρ_0 is the ion number density at the center of the cell, k is the Boltzmann constant, P_θ the canonical angular momentum, and the integration is over momentum space. One can estimate the nonuniformity of the radial distribution by assuming the electrostatic potential is separable, $V(r,z)=V(r)+V(z)$. Then the charge density becomes [32]

$$\rho(r,z)\sim\rho_0\exp\left\{\frac{-m}{2kT_i}\left(\Gamma r^2+\frac{2q}{m}V(z)\right)\right\} \quad r<r_P$$
$$\rho(r,z)\equiv 0 \qquad r>r_P \tag{18}$$

where Γ is the line width of the ICR signal. For harmonic trapping potentials, $V(z)\propto z^2$, the charge distribution is Gaussian along both r and z. Experimentally, Γ is small; thus, the radial charge distribution is nearly uniform. A uniform radial distribution has been observed experimentally for electrons in pure electron plasmas confined in devices of similar geometry [33]. Ions are produced initially from neutral gas in the cell by electron ionization, which initially localizes the ion cloud along the electron beam in a cylinder with a radius defined by the electron beam and the ion cyclotron radius. Thus, initially the ions form a prolate ellipsoid with uniform density. As the ions thermalize and expand radially due to ion/neutral species collisions, the charge distribution remains an ellipsoid of near-uniform density, and the eccentricity and density evolve with time.

In 1842 Thomson [34] analyzed the electrostatic potential of a uniform ellipsoidal charge distribution, and showed that inside the distribution the potential was given by

$$V_{SC}(x,y,z)=-\frac{q\rho}{2\epsilon_0}\left[G_{ix}x^2+G_{iy}y^2+G_{iz}z^2\right] \tag{19}$$

where G_{ix}, G_{iy}, and G_{iz} are geometric factors. Applying Poisson's equation to (19),

$$G_{ix}+G_{iy}+G_{iz}=1 \tag{20}$$

If the semi-major axes of our ellipsoid are aligned with the coordinate system as shown in Fig. 2(a), with $y_0>z_0>x_0$, two eccentricities are defined

$$\xi\equiv\left(1-z_0^2/y_0^2\right)^{1/2} \tag{21}$$

and

$$\xi' \equiv \left(1 - x_0^2/y_0^2\right)^{1/2} \tag{22}$$

The geometric factors are given by [34]

$$G_{i_y} = \left(1 - \xi^2\right)^{1/2}\left(1 - \xi'^2\right)^{1/2}\int_0^1 \frac{u^2 \mathrm{d}u}{\left(1 - \xi^2 u^2\right)^{1/2}\left(1 - \xi'^2 u^2\right)^{1/2}} \tag{23}$$

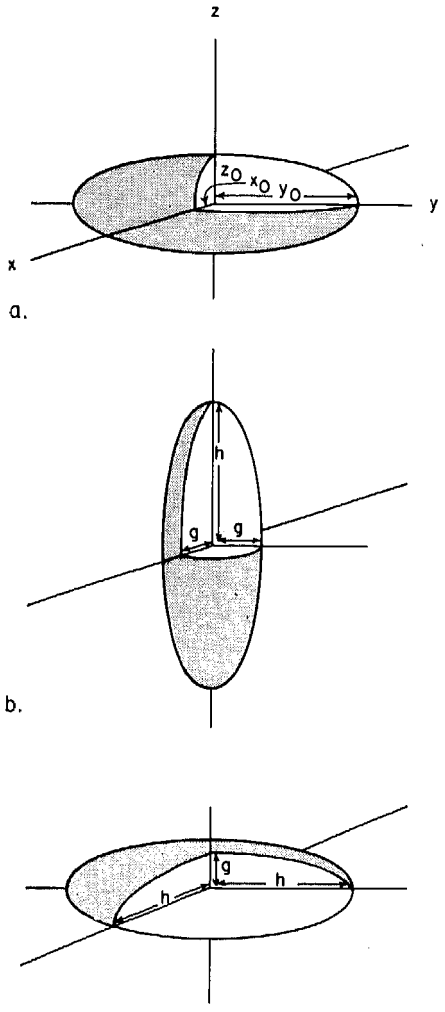

Fig. 2. Ellipsoids: (a) general ellipsoid with $y_0 > z_0 > x_0$; (b) prolate spheroid, $h > g$; (c) oblate spheroid with $h > g$.

$$G_{iz} = (1-\xi^2)^{1/2}(1-\xi'^2)^{1/2}\int_0^1 \frac{u^2 du}{(1-\xi^2u^2)^{3/2}(1-\xi'^2u^2)^{1/2}} \tag{24}$$

and

$$G_{ix} = (1-\xi^2)^{1/2}(1-\xi'^2)^{1/2}\int_0^1 \frac{u^2 du}{(1-\xi^2u^2)^{1/2}(1-\xi'^2u^2)^{3/2}} \tag{25}$$

For the general case the integrals must be evaluated numerically; however, the special geometries of ion trapping instruments give rise to simplifications. In the "Penning" trap or cubical ICR cell, the ion cloud will initially be a prolate spheroid oriented along the magnetic field (see Fig. 2(b)). In the usual operating condition of $qV \gg kT$, this charge distribution will evolve from prolate to oblate as the cloud cools and expands by collisions with the background neutral gas (see Fig. 2(c)). In the elongated ICR cell the ion cloud will remain prolate. The case of the rectangular ICR cell is more complex, and it will be considered separately later.

Penning, cubical and elongated cells

For both the prolate and oblate spheroid cloud geometries, the ellipsoid equations are degenerate. Equation (19) can be written

$$V_{SC}(x, y, z) = \frac{-q\rho}{2\epsilon_0}\left[G_i(x^2+y^2) + G_{iz}z^2\right] \tag{26}$$

where G_i for the prolate case is given by

$$G_i = 1/(2\xi^2) - \{(1-\xi^2)/(2\xi^2)\}\tanh^{-1}\xi \tag{27}$$

and G_i for the oblate case is given by

$$G_i = (1-\xi^2)^{1/2}/(2\xi^2)\left\{\left(\frac{1}{\xi}\sin^{-1}\xi - (1-\xi^2)^{1/2}\right)\right\} \tag{28}$$

Here ξ is given by

$$\xi = \left[1 - g^2/h^2\right]^{1/2} \tag{29}$$

where h is the larger semi-major axis and g the smaller (see Fig. 2). The quantity G_i is evaluated and plotted in Fig. 3 as the shape goes from extreme prolate (infinitely long rod) to extreme oblate (infinitesimally thin disk).

To calculate the ICR frequency one need only consider the x and y components of the space-charge electric field. Using eqn. (26) for the space-charge potential and adding it to the applied trapping potential, a space-charge modified K' analogous to eqn. (7) is obtained

$$K' = \frac{q}{m}\left(\frac{E_r}{r}\right) = \frac{2qVG_T}{m} + \frac{q^2\rho G_i}{\epsilon_0 m} \tag{30}$$

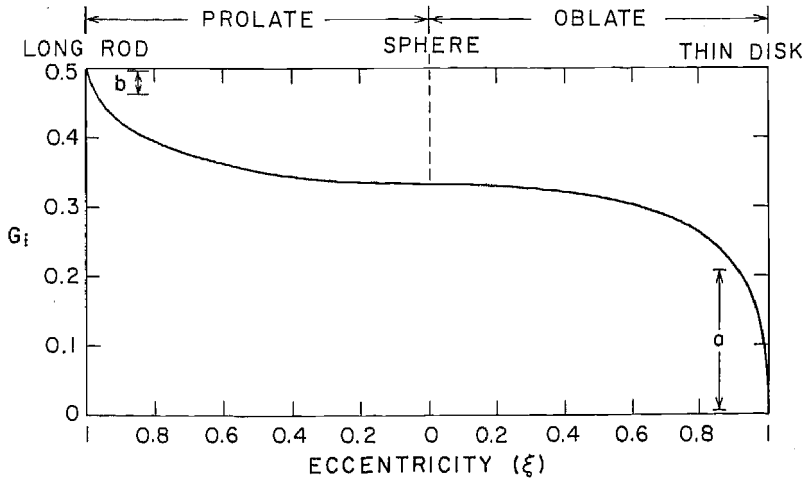

Fig. 3. Ion cloud geometry factors for eqn. (31). Region a shows the range of G_i for typical operating parameters in the "Penning" and cubical ICR geometries. Region b shows the range for the elongated ICR.

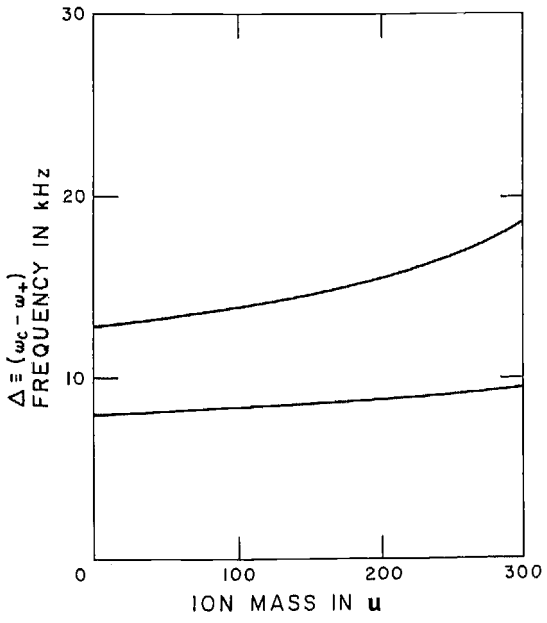

Fig. 4. Δ vs. mass for the "Penning" trap ($r_0 = 0.625$ cm, $z_0 = 0.38$ cm) with $V = 2$ V, $B = 1.175$ T. The lower curve is for a single particle and the upper curve is when $\rho G_i = 10^6$ cm^{-3}.

where E_r is the radial component of the electric field. This K' is inserted into eqns. (11) and (12) to give the space-charge modified eigenfrequencies

$$\omega_{\pm} = \frac{\omega_c}{2}\left\{1 \pm \left[1 - 4\left(2qVG_T/m + \rho q^2 G_i/\epsilon_0 m\right)/\omega_c^2\right]^{1/2}\right\} \tag{31}$$

To demonstrate the magnitude of the space-charge influence in eqn. (31), Fig. 4 shows a plot of $\Delta \equiv \omega_c - \omega_+$ in the Penning trap with $V = 2V$ and $B = 1.175$ T. The lower curve shows the weak mass dependence of this difference for the single ion solution of eqn. (12). The upper curve indicates the influence on ω_+ for an ion number density of 1×10^6 cm^{-3}. Before considering additional implications of eqn. (31), the above development is repeated here for the rectangular ICR cell.

Rectangular ICR cell

Sharp et al. [28] have shown that eqn. (3) describes the electrostatic potential in the rectangular ICR cell ($a = c < b$) near its center, where $\alpha \neq \beta$. For this case, the single particle Lagrangian for motion in the x–y plane for sufficiently small values of x and y is

$$L = \tfrac{1}{2}m\left(\dot{x}^2 + \dot{y}^2\right) + \tfrac{1}{2}mK_x x^2 + \tfrac{1}{2}mK_y y^2 + \tfrac{1}{2}m\omega_c\left(\dot{y}x - \dot{x}y\right) \tag{32}$$

where K_x and K_y are analogous to the K of eqn. (7). While the equations of motion are messy, the algebra is straightforward. Using the same methods for eqn. (6), the eigenfrequencies are

$$\omega_{\pm} = \frac{\omega_c}{\sqrt{2}}\left\{1 - \frac{K_x + K_y}{\omega_c^2} \pm \left[1 - \frac{2\left(K_x + K_y\right)}{\omega_c^2} + \frac{\left(K_x - K_y\right)^2}{\omega_c^4}\right]^{1/2}\right\}^{1/2} \tag{33}$$

If eqn. (3) were valid for values of x and y nearly out to the cell walls, as it is for the cubical and elongated ICR systems, then by analogy with the previous development, one could incorporate space-charge in the model by writing

$$K_x = \frac{2qV_T}{m}G_{Tx} + \frac{q^2\rho}{\epsilon_0 m}G_{ix} \tag{34}$$

and

$$K_y = \frac{2qV_T}{m}G_{Ty} + \frac{q^2\rho}{\epsilon_0 m}G_{iy} \tag{35}$$

where G_{Tx} and G_{Ty} are given in Table 1. The G_i terms are as discussed above for the general ellipsoid which should be a good approximation of the ion cloud's shape [see Fig. 2(a) and eqns. (19)–(25)].

Unfortunately, in rectangular ICR cells there is a significant fraction of the ion density in regions where eqn. (3) is not expected to be valid. For example, in a typical ICR cell ($a = c = 2.54$ cm, $b = 8.89$ cm) with an applied potential of 0.5 V, ion densities as high as 1.5×10^5 cm^{-3} are possible [16], and ion numbers as great as 5×10^5 have been measured [35]. Thus, the ions fill more than 3 cm^3, and the ion cloud must extend nearly 3 cm in the y direction. This is well beyond the limits of validity [28] for the harmonic potential approximation of eqn. (3). However, highly symmetric ICR signals of narrow spectral width (< 500 Hz) are observed even for large numbers of ions [2–4,35]. This implies that the space-charge modified potential must remain harmonic. Were anharmonic terms of any great importance, we would expect severe power broadening and asymmetrization of the fundamental resonance line to occur [29].

A phenomenological model for a harmonic potential in the rectangular ICR cell can be constructed starting from the approximation to the trapping potential given by [28]

$$V_{\text{Trap}}(x, y, z) = \frac{1}{2}(V_{\text{T}} + V_0) + V\left[-\frac{\alpha}{a^2}x^2 - \gamma \cosh\left(\frac{\eta y}{b}\right) + \frac{\delta}{a^2}z^2\right] \tag{36}$$

which is valid over a larger spatial extent. The constants have been calculated [28] to be $\alpha = 2.185$, $\gamma = 6.97 \times 10^{-4}$, $\eta = 15.4$, $\delta = 2.192$, with a and b as given in Table 1. Assuming that the space-charge potential field is given by

$$V_{\text{SC}}(x, y, z) = -q\rho/2\epsilon_0 G_{\text{i}x}x^2 - q\rho/2\epsilon_0 G_{\text{i}y}y^2 - \frac{1}{2}V\gamma\left(\frac{\eta}{b}\right)^2 y^2 + V\gamma \cosh\left(\frac{\eta y}{b}\right) - q\rho/2\epsilon_0 G_{\text{i}z}z^2 \tag{37}$$

adding (36) and (37), one obtains

$$V(x, y, z) = \frac{1}{2}(V_{\text{T}} + V_0) + \left[-\left(V\frac{\alpha}{a^2} + q\rho/2\epsilon_0 G_{\text{i}x}\right)x^2 - \left(\frac{V\beta}{b^2} + q\rho/2\epsilon_0 G_{\text{i}y}\right)y^2 + \left(\frac{V\delta}{a^2} - q\rho/2\epsilon_0 G_{\text{i}z}\right)z^2\right] \tag{38}$$

which is harmonic. Equation (37) is, of course, only a construct which allows us to explain the data, and not a result from first principles. However, the apparent stability of the ion charge distribution against the occurrence of plasma instabilities indicates [32] that the radial electric field with space-charge is monotonically increasing as in our construct.

The relationship between $G_{\text{i}x}$ and $G_{\text{i}y}$ for the rectangular ICR cell can be established by requiring that the radial space-charge field is everywhere parallel to that of the cell. This is justified by two facts. First, the drift

trajectory at frequency ω_- is nearly mass independent, and second, the effect of ion space-charge on the ICR frequency is observed empirically to be qualitatively the same as a change in applied potential [7]. With this model, eqn. (22) becomes

$$\xi' = \left(1 - G_{Ty}/G_{Tx}\right)^{1/2} \tag{39}$$

or for the particular rectangular ICR listed in Table 1, $\xi' = 0.9984$. The space-charge terms are related by

$$G_{ix} = \frac{G_{Tx}}{G_{Ty}} G_{iy} \tag{40}$$

Thus, the possible range of cloud geometry factors can be parameterized by a single variable, ξ, and Fig. 5 gives the range of ion cloud geometry factors, G_{iy}, for the rectangular ICR cell calculated from eqn. (23) using $\xi' = 0.9984$.

TEMPORAL EVOLUTION OF THE ICR FREQUENCY

Equations (31) and (33) give the observed ICR frequency with the ion space-charge contribution reduced to a single parameter, ρG_i (or ρG_{iy}). This parameter is the product of an ion cloud geometry factor and the ion density, both of which evolve in time. The equilibrium dimension of the ion cloud along the z direction can be estimated [16] making use of the fact

$$kT_i/2 \approx \left(qVG_{Tz} - \frac{q^2\rho}{2\epsilon_0} G_i\right) z^2 \tag{41}$$

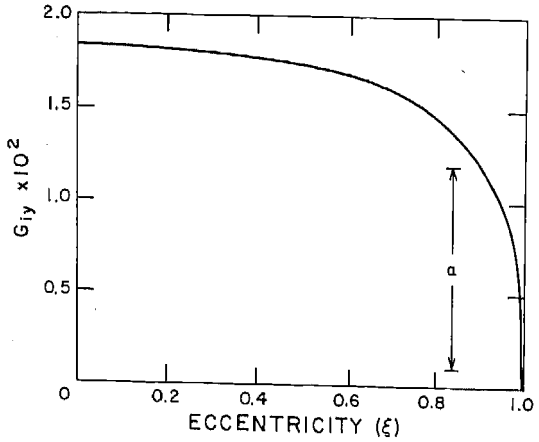

Fig. 5. Ion cloud geometry factors for eqns. (35), (40) and (42), from eqn. (23) with $e' = 0.9984$. Region a shows the range of G_{iy} for typical operating parameters in the rectangular ICR cell.

As the applied potential V is increased and T_i is decreased, the ion cloud becomes localized in the z direction (oblate, $\xi \rightarrow 1$). In the limit $z \rightarrow 0$, we see from Figs. 3 and 5 that the geometry factor vanishes and hence so does the space-charge shift of $\omega_{+/-}$. To minimize the space-charge shift in all but the elongated geometries, one minimizes the ion temperature and maximizes the applied trapping potential. However, this also maximizes the ion density, ρ. As the ion cloud is localized, the number of ions must be reduced to maintain the same ion density. We also note that increasing V increases the value of ω_-, giving a larger applied potential shift to the observed ICR frequency.

The time evolution of the ion cloud in its approach to thermal equilibrium with the instrument is governed by ion–ion collisions as well as by ion/neutral species collisions. The ion–ion self-equilibration rapidly establishes a Boltzmann distribution of ion energies [16,36]. Those ions in the high energy tail of this distribution with energy greater than the trapping potential energy "evaporate" along the z axis. This process cools the ion cloud to less than 15% of the well depth (qV) in less than 25 s. Cooling of the ions to thermal equilibrium with the instrument occurs at the ion/neutral collision rate ($\sim$ 1 s at 10^{-5} Pa).

After the evaporative cooling phase, charge loss is due only to collisional radial transport across the magnetic field, though some ions may undergo reactions with the background gas, thus changing q/M. The ion density, ρ, will then decrease in time as the ion cloud expands. There are two competing collisional processes that provide radial transport: diffusion and collisional mobility [37]. However, both of these mechanisms give confinement times which scale as B^2/p, where p is the neutral pressure in the instrument. By increasing the trapping time, the ion density evolves more slowly and the ICR frequency changes more slowly. Trapping time may be increased by lowering the pressure, but at the expense of increasing the thermal equilibration time.

We have observed this temporal evolution of the ion frequencies in the Penning trap. In our instrument, observation of $\omega_{+/-}$ requires active detection techniques, where the ions are driven in an applied r.f. electric field similar to ICR detection techniques [38]. These active detection schemes perturb the quiescent ion cloud evolution. Alternatively, we can bolometrically observe the motion along the z axis in the electrostatic potential well without perturbing the ion motion [36]. The frequency of single particle motion given in eqn. (5) is also perturbed by space-charge and is given by

$$\omega_z' \approx \left(\frac{2qVG_{T_z}}{m} - \frac{q^2 \rho G_{iz}}{\epsilon_0 m} \right)^{1/2} \tag{42}$$

where G_{iz} is given by eqn. (20). Figure 6 shows the evolution of $\nu = \omega_z/2\pi$ as

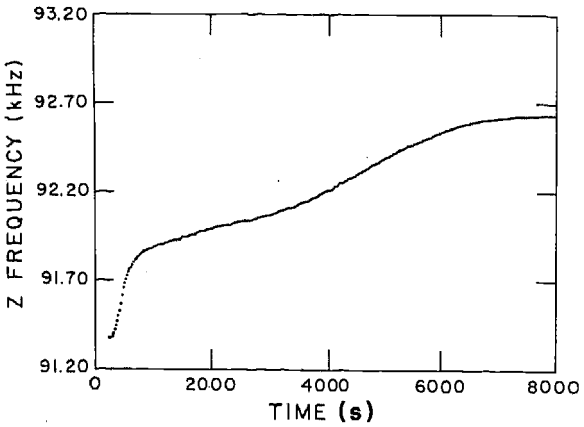

Fig. 6. Time evolution of ν_z in the "Penning" trap ($r_0 = 0.625$ cm, $z_0 = 0.38$ cm) with $m = 30$ u, $V = 2$ V, $B = 1.175$ T.

a function of time for NO^+ ions with a background pressure of 1.3×10^{-8} Pa (1×10^{-10} Torr) composed primarily of NO and H_2. The ion trap was of the Penning configuration shown in Fig. 1(a), with 2 V applied between end cap and ring. Initially the large loss of ions due to the evaporative cooling process lowers the ion density and alters the geometry factor. This is followed by the slower reduction in ion density due to radial transport of the ions. This radial evolution of the ion cloud was observed to be altered by changes in background density and composition as expected from a confinement time inversely proportional to the collision rate [16]. Although these measurements refer to ω_z, the evolution is due to the ion space-charge, ρG_i, which is common to eqns. (31) and (33) for $\omega_{+/-}$. Temporal shifts in ω_+ for an ICR cell have been clearly observed by Francl et al. [11].

DISCUSSION

It is emphasized again that the shifts predicted by eqn. (31) for Penning traps and ICR cells with $a = b$, and by eqn. (33) for rectangular ICR cells will be observed only if the instrument antennae detect or excite single particle motions as opposed to center-of-mass motions. This is a common situation as discussed earlier in this paper.

There are several implications of this model for the influence of ion space-charge on ICR frequency. Using eqn. (41) along with independent measurements [2–4,5,28,38] of ion number and density, one can estimate the ranges of geometric factors that are likely to occur for ion clouds in various instruments; these ranges are bracketed by regions a and b in Fig. 3, and

region *a* in Fig. 5. The geometric factor for the ion cloud in Penning, cubical, and rectangular ICR cells is a very strong function of the shape of the cloud in normal operating conditions. For the new elongated ICR cell, the range of the ion cloud geometric factor is limited, but the absolute value is 2–10 times greater. Hence influence of space-charge for a given density is greater. The applied potentials in this instrument [27] are similar to those used in conventional cells [2–4], while the dimensions are much greater. This makes the trap geometric factors smaller, resulting in much smaller electric fields. The space-charge frequency shift in the elongated cell will be larger or comparable to the conventional cell, but it will vary over a smaller range as the cloud evolves.

For precision mass spectroscopy in ICR cell instruments, it is important to calibrate and make measurements at the same point in the temporal evolution in the ion cloud. This requires that the same neutral background pressure and composition be maintained, as well as the same values of magnetic field, electrostatic well depth, and measurement time. To insure the same initial ion cloud size and shape, the ionization conditions of electron current and duration need to be controlled, and the evolution time from ion production to mass measurement must be kept constant. Finally, as is well known, increasing the magnetic field increases the confinement time and slows the temporal evolution. Independent measurements of all ion eigenfrequencies (ω_z', ω_+, ω_-) and other techniques to characterize the ion cloud, such as measurement of total charge [11,27], will improve the confidence of precision ICR mass calibrations using eqns. (31) or (33).

Francl et al. [11] have observed the ion density effects of eqns. (31) and (33). They have made use of the knowledge of the functional dependences to calibrate their instruments to give relative mass measurements to better than 1 p.p.m. and absolute mass measurements to the order of 10 p.p.m. Other similar measurements have previously been reported by Locke [39].

ACKNOWLEDGMENTS

We wish to thank Professor William Allis, JILA Visiting Fellow in 1979–80 and Professor Robert T. McIver, Jr., JILA Visiting Fellow in 1978–79, for much encouragement and many illuminating discussions. This work was supported in part by National Science Foundation grants PHY79-04928 and PHY82-00805 through the University of Colorado.

REFERENCES

1 F.M. Penning, Phys., 3 (1936) 873.
2 J.L. Beauchamp, Annu. Rev. Phys. Chem., 22 (1971) 527.

3 H. Hartmann and K.P. Wanczek (Eds.), Ion Cyclotron Resonance Spectrometry, Springer–Verlag, Berlin, 1978.
4 T.A. Lehman and M.M. Bursey (Eds.), Ion Cyclotron Resonance Spectrometry, Wiley, New York, 1976.
5 R.T. McIver, Jr. and A.D. Barangi, Int. J. Mass Spectrom. Ion Phys., 14 (1974) 449.
6 E.B. Ledford Jr. and R.T. McIver, Jr., Int. J. Mass Spectrom. Ion Phys., 22 (1976) 399.
7 E.B. Ledford Jr., S. Ghaderi, R.L. White, R.B. Spencer, P.S. Kulkarni, C.L. Wilkins and M.L. Gross, Anal. Chem., 52 (1980) 463.
8 M.B. Comisarow and A.G. Marshall, Chem. Phys. Lett., 25 (1974) 282.
9 A.G. Marshall and M.B. Comisarow, Anal. Chem., 47 (1975) 491A.
10 M.B. Comisarow and A.G. Marshall, J. Chem. Phys., 62 (1975) 293.
11 T.J. Francl, M.G. Sherman, R.L. Hunter, M.J. Locke, W.D. Bowers and R. McIver, Jr., Int. J. Mass Spectrom. Ion Phys., in press.
12 D.J. Wineland, J.J. Bollinger and W.M. Itano. Phys. Rev. Lett., 50 (1983) 623.
13 D.J. Wineland and H.G. Dehmelt, J. Appl. Phys., 46 (1975) 919.
14 D.J. Wineland and H.G. Dehmelt, Int. J. Mass Spectrom. Ion Phys., 16 (1975) 338.
15 See, for some examples, ref. 12; F.L. Walls, Ph.D. Thesis, University of Washington, Seattle, 1970, unpublished, available through University Microfilms, Inc., Ann Arbor, MI; F.L. Walls and T.S. Stein, Phys. Rev. Lett., 31 (1973) 975; ref. 36.
16 J.B. Jeffries, Ph.D. Thesis, University of Colorado, Boulder, CO, 1980.
17 F.L. Walls and G.H. Dunn, J. Geophys. Res., 79 (1974) 1911.
18 R.A. Heppner, F.L. Walls, W.T. Armstrong and G.H. Dunn, Phys. Rev. A, 13 (1976) 1000.
19 R.D. DuBois, J.B. Jeffries and G.H. Dunn, Phys. Rev. A, 17 (1978) 1314.
20 J. Luine, Ph.D. Thesis, University of Colorado, Boulder, CO, 1981; J.A. Luine and G.H. Dunn, Book of Abstracts, XII Int. Conf. on the Physics of Electronic and Atomic Collisions, Gatlinburg, TN, 1981, p. 1035.
21 J. Byrne and P.S. Fargo, Proc. Phys. Soc. London, 86 (1965) 801.
22 H.G. Dehmelt, in D.R. Bates and J. Esterman (Eds.), Advances in Atomic and Molecular Physics, Academic Press, New York, 1967, Vol. 3, p. 53; 1969, Vol. 5, p. 109.
23 H.G. Dehmelt, in D. Kleppner and F.M. Pipkin (Eds.), Atomic Physics, Plenum, New York, 1981, Vol. 7, p. 337.
24 R.S. Van Dyck Jr., P.B. Schwinberg and H.G. Dehmelt, in B.M. Kursunoglu, A. Perlmutter and L.F. Scott (Eds.), New Frontiers in High Energy Physics, Plenum, New York, 1978, p. 159.
25 D.J. Wineland, R.E. Drullinger and F.L. Walls, Phys. Rev. Lett., 40 (1978) 1639.
26 For a recent review of spectroscopic applications, see: D.J. Wineland, in D.R. Bates and B. Bederson (Eds.), Advances in Atomic and Molecular Physics, Academic Press, New York, 1983, Vol. 19, pp. 135–186.
27 R.L. Hunter, M.G. Sherman and R.T. McIver, Jr., Int. J. Mass Spectrom. Ion Phys., 50 (1983) 259.
28 T.E. Sharp, J.R. Eyler and E. Li, Int. J. Mass Spectrom. Ion Phys., 9 (1972) 421.
29 L.D. Landau and E.M. Lifshiftz, Mechanics, Pergamon Press, Oxford, 1976, 3rd edn; sections 28 and 29 contain a readable discussion of anharmonic effects in harmonic oscillators.
30 P. Ekstrom and D. Wineland, Sci. Am., 243 (1980) 104.
31 J.L. Beauchamp and J.T. Armstrong, Rev. Sci. Instrum., 40 (1969) 123.
32 R.C. Davidson, Theory of Non-neutral Plasma, W.H. Benjamin, New York, 1979.
33 J.S. de Grassie and J.H. Malmberg, Phys. Fluids, 23 (1980) 63.

34 W. Thomson, Cambridge Math. J., 3 (1842) 71; also in Reprint of Papers on Electrostatics and Magnetism, Macmillan, London, 1884 2nd edn., p. 1.
35 R.T. McIver, Jr., private communication, 1982.
36 H.G. Dehmelt and F.L. Walls, Phys. Rev. Lett., 21 (1968) 127.
37 W.P. Allis, in S. Flugge (Ed.), Handbuch der Physik, Springer-Verlag, Berlin, 1956, Vol. 21, p. 383.
38 R.T. McIver, Jr., E.D. Ledford, Jr. and R.L. Hunter, J. Chem. Phys., 72 (1980) 2535.
39 M. Locke, Ph.D. Thesis, University of California, Irvine, CA, 1981.